Glycobiology vol. 22 no. 8 pp. 1103–1117, 2012
doi:10.1093/glycob/cws080
Advance Access publication on May 3, 2012

Localization and structural analysis of a conserved pyruvylated epitope in *Bacillus anthracis* secondary cell wall polysaccharides and characterization of the galactose-deficient wall polysaccharide from avirulent *B. anthracis* CDC 684

L Scott Forsberg[1,2], Teresa G Abshire[3], Arthur Friedlander[4], Conrad P Quinn[5], Elmar L Kannenberg[2], and Russell W Carlson[2]

[2]Complex Carbohydrate Research Center, University of Georgia, 315 Riverbend Road, Athens, GA 30602, USA; [3]Diagnostic Systems Division, and [4]Headquarters Division, United States Army Medical Research Institute of Infectious Diseases, 1425 Porter Street, Frederick, MD 21702, USA; and [5]Centers for Disease Control and Prevention, 1600 Clifton Road, Atlanta, GA 30333, USA

Received on February 17, 2012; revised on April 25, 2012; accepted on April 26, 2012

Bacillus anthracis **CDC 684 is a naturally occurring, avirulent variant and close relative of the highly pathogenic *B. anthracis* Vollum. *Bacillus anthracis* CDC 684 contains both virulence plasmids, pXO1 and pXO2, yet is non-pathogenic in animal models, prompting closer scrutiny of the molecular basis of attenuation. We structurally characterized the secondary cell wall polysaccharide (SCWP) of *B. anthracis* CDC 684 (Ba684) using chemical and NMR spectroscopy analysis. The SCWP consists of a HexNAc trisaccharide backbone having identical structure as that of *B. anthracis* Pasteur, Sterne and Ames, →4)-β-D-Man*p*NAc-(1 → 4)-β-D-Glc*p*NAc-(1 → 6)-α-D-Glc*p*NAc-(1→. Remarkably, although the backbone is fully polymerized, the SCWP is the devoid of all galactosyl side residues, a feature which normally comprises 50% of the glycosyl residues on the highly galactosylated SCWPs from pathogenic strains. This observation highlights the role of defective wall assembly in virulence and indicates that polymerization occurs independently of galactose side residue attachment. Of particular interest, the polymerized Ba684 backbone retains the substoichiometric pyruvate acetal, *O*-acetate and amino group modifications found on SCWPs from normal *B. anthracis* strains, and immunofluorescence analysis confirms that SCWP expression coincides with the ability to bind the surface layer homology (SLH) domain containing S-layer protein extractable antigen-1. Pyruvate was previously demonstrated as part of a conserved epitope, mediating SLH-domain protein attachment to the underlying peptidoglycan layer. We find that a single repeating unit, located at the distal (non-reducing) end of the Ba684 SCWP, is structurally modified and that this modification is present in identical manner in the SCWPs of normal *B. anthracis* strains. These polysaccharides terminate in the sequence: (S)-4,6-*O*-(1-carboxyethylidene)-β-D-Man*p*NAc-(1 → 4)-[3-*O*-acetyl]-β-D-Glc*p*NAc-(1 → 6)-α-D-Glc*p*NH_2-(1→.**

Keywords: Bacillus anthracis / cell wall / polysaccharide / pyruvylation / structure

Introduction

Attenuated strains of *Bacillus anthracis* are of continuing interest as a basis for vaccine preparation and the study of anthrax etiology. *Bacillus anthracis* CDC 684 is a naturally occurring, avirulent strain which resides within the *B. anthracis* phylogenetic tree, in close proximity to *B. anthracis* Pasteur, Sterne and the highly pathogenic Ames strain (Okinaka et al. 2011). Until recently, this strain went largely unnoticed, mainly because it was originally classified as *Bacillus megaterium* CDC 684/NRRL-349S/NRS234 (Ezzell et al. 1990). This classification was generally attributed to its lack of pathogenicity and failure to react with a monoclonal antibody (EAII6G6) directed to a shared polysaccharide antigen common to known *B. anthracis* strains (Ezzell et al. 1990). Re-examination of this strain resulted in re-classification as *B. anthracis* CDC 684 (Ba684; Ezzell et al. 1990) based on several phenotypic traits shared with *B. anthracis*, including the production of poly-D-glutamic acid capsule and protective antigen, sensitivity to γ-bacteriophage, non-motility and non-hemolytic on blood agar, all hallmarks of the *B. anthracis* phenotype (Ezzell et al. 1990; Abshire et al. 2005). *Bacillus anthracis* CDC 684 contains what appears to be intact forms of both virulence plasmids, pXO1 and pXO2, yet is non-pathogenic in animal models, prompting closer scrutiny of the molecular basis of attenuation (Okinaka et al. 2011). A recent

[1]To whom correspondence should be addressed: Tel: +1-706-542-4479; Fax: +1-706-542-4412; e-mail: sforsb@ccrc.uga.edu

detailed analysis of the Ba684 genome (Okinaka et al. 2011), together with comparative whole genome sequencing (Pearson et al. 2004), revealed that it belongs to the highly virulent *B. anthracis* A lineage, where it differs from the pathogenic *B. anthracis* Vollum by only 51 single-nucleotide polymorphisms (SNPs). *Bacillus anthracis* CDC 684 also contains a large chromosomal inversion (3.3 Mbp) resulting in displacement of the relative orientation of the origin (*ori*) and termination (*ter*) of replication (Keim et al. 2009; Okinaka et al. 2011). The authors hypothesized that either one or both of these chromosomal differences (i.e. chromosomal inversion or 51 SNPs unique to Ba684) could account for the lack of lethality of this organism, as well as its altered (slower) growth kinetics in culture (Okinaka et al. 2011).

The *B. anthracis* cell wall comprises an extensive peptidoglycan (PG), which underlies an exterior coating of S-layer protein (Fouet 2009). Another component, the secondary cell wall polysaccharide (SCWP), is a class of low-molecular-weight polysaccharides that serve unique and specific functions. The SCWPs are covalently linked at their reducing end to PG muramic acid residues by phosphate esters (Schäffer and Messner 2005; Choudhury et al. 2006; Fouet 2009). Several studies have demonstrated that SCWPs facilitate anchoring and/or targeting of proteins to the cell surface, including the S-layer proteins, through non-covalent interactions with a conserved domain in these proteins, the surface layer homology (SLH) domain (Mesnage et al. 1999, 2000; Cava et al. 2004; Kern et al. 2010). These studies also demonstrated that pyruvate acetal, carried on the polysaccharide at an undefined location, is an essential component of the epitope recognized by the SLH domain (Mesnage et al. 2000; Schäffer and Messner 2005; Kern et al. 2010).

Recently, we described the glycosyl structures of the SCWPs from *B. anthracis* Ames, Sterne and Pasteur and from phylogenetically related strains of pathogenic *Bacillus cereus* (Choudhury et al. 2006; Forsberg et al. 2011). The SCWPs from all of these strains share a common backbone which comprises a HexNAc trisaccharide repeating unit, →4)-β-D-Man*p*NAc-(1 → 4)-β-D-Glc*p*NAc-(1 → 6)-α-D-Glc*p*NAc-(1→, and all are highly substituted at specific locations with galactose side residues in α- and β-linkages, the locations and degree of galactosylation being species/strain-specific. Additionally, we observed that the isolated SCWPs from *B. anthracis* are highly immunogenic (Leoff et al. 2009) and that the chromatographically purified polysaccharides carry the epitope recognized by MAb EAII6G6 (N. Kamal et al. in preparation), used routinely to identify and distinguish *B. anthracis* whole cells (Ezzell et al. 1990; De et al. 2002). Recently, we found that the SCWP from pathogenic *B. anthracis* is the ligand for the carbohydrate-binding domains of the *B. anthracis* phage endolysins, PlyG and PlyL (J. Ganguly et al. submitted). In view of the aforementioned genetic characteristics of Ba684, its unexplained lack of pathogenicity and its failure to react with the *B. anthracis*-specific MAb EAII6G6 (Ezzell et al. 1990), we were interested to examine the nature of any SCWP synthesized by this organism.

In the present study, we show that Ba684 does indeed polymerize an SCWP, which can be released from PG using hydrofluoric acid (HF). Remarkably, although the glycosyl backbone is fully polymerized, the SCWP is totally devoid of all galactose side chains (both α- and β-linked), a feature which normally comprises 50% of the glycosyl residues of the highly galactosylated SCWPs from pathogenic strains. This finding may help account for the extensive heterogeneity in side residue attachment in the SCWPs from these strains of *B. anthracis* and related *B. cereus* (Choudhury et al. 2006; Leoff et al. 2008; Forsberg et al. 2011). Moreover, structural alterations of this magnitude could result in defective wall assembly, possibly contributing to the altered growth kinetics and virulence properties of this strain.

In normal pathogenic *B. anthracis*, pyruvate acetal, linked to a carrier wall polysaccharide at an undefined location, was previously demonstrated to be an essential part of an epitope mediating the adhesion of the SLH-domain proteins to the exterior of PG (Mesnage et al. 2000; Fouet 2009; Kern et al. 2010). However, in these normal *B. anthracis* strains, the complete glycosyl epitope containing pyruvate could not be localized or structurally defined, due to the substoichiometric nature of the pyruvate modification and the complexity of NMR spectra resulting from multiple sites of galactosylation. Since the Ba684 SCWP lacks all galactosyl residues, the weak substoichiometric NMR signals arising from the non-repeating pyruvate modification are no longer masked, allowing for the first time complete structural elucidation of the non-repeating, pyruvylated epitope and adjacent structural modifications. Moreover, structural definition of the epitope in Ba684 has facilitated identification of several unique reporter signals, detectable in the normal pathogenic *B. anthracis* SCWPs, allowing the localization of a conserved pyruvylated epitope in these SCWPs from normal, pathogenic *B. anthracis* and related pathogenic *B. cereus*. We find that these SCWPs are *O*-acetylated and *N*-deacetylated at specific HexNAc residues, adjacent to the pyruvylated residue.

Results

Demonstration of the S-layer on avirulent Ba684 whole cells

Whole cells of *B. anthracis* Sterne $34F_2$, and the avirulent Ba684, were examined for the presence of the S-layer by immunolabeling with antiserum raised to the S-layer protein EA1 (extractable antigen-1; Farchaus et al. 1995). As shown in Figure 1, this protein marker for the S-layer was detected on both the representative pathogenic strain and the avirulent Ba684 strain, a strong indicator that both of these strains express the pyruvylated cell wall epitope which mediates SLH-domain protein attachment. The exact location of pyruvate on SCWPs and detailed structural features of adjacent glycosyl residues are described in the following sections. The presence of an S-layer on the well-studied Ames, Pasteur and Sterne strains has already been demonstrated (Fouet 2009).

In a separate experiment, cells of Sterne $34F_2$ were simultaneously incubated with the anti-EA1 antiserum and the anti-glycosyl monoclonal antibody EAII6G6, shown previously to be directed to the *B. anthracis* common SCWP (Ezzell et al. 1990). As shown in Figure 2B, EAII6G6 reactivity on mature cells appeared as a patchy surface pattern with gaps, which precisely (i.e. inversely) complemented the reactivity pattern

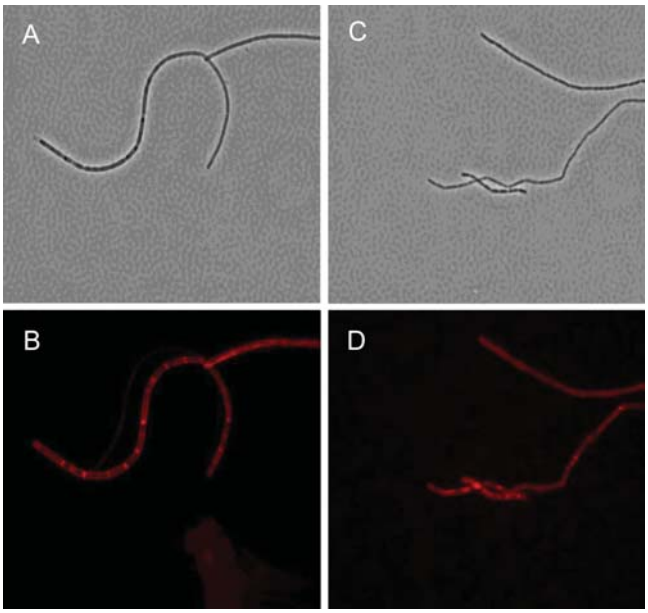

Fig. 1. Demonstration of S-layer coat by immunofluorescence labeling of whole cells of *B. anthracis* with anti-S-layer EA1 antiserum. (**A** and **B**) Phase contrast and fluorescence microscopy of *B. anthracis* Sterne 34F$_2$; (**C** and **D**) the identical analysis applied to Ba684. Non-encapsulated *B. anthracis* strains possess a proteinaceous S-layer coating, and the avirulent Ba684 strain is no exception, evidenced here by immunodetection of the specific S-layer protein EA1 in both a typical pathogenic strain and the CDC 684 strain. Immunodetection was performed using the ATTO594-secondary conjugate anti-EA1 antiserum.

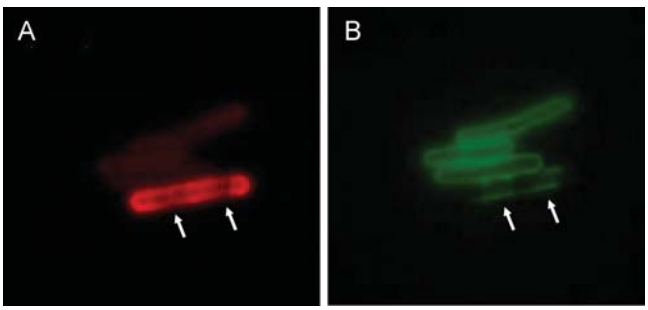

Fig. 2. Differential staining of S-layer protein EA1, and SCWP, on the *B. anthracis* Sterne cell surface. (**A**) Cells visualized with ATTO594-anti-EA1. In the bottom brightly fluorescent cell, recognition of the S-layer protein EA1 reveals a specific localization pattern of nascent S-layer deposition. The gaps in staining (arrows) indicate an absence of S-layer probably due to incomplete deposition. The upper three cells (young cells) show only weak staining with anti-EA1 reflecting very early stages of S-layer synthesis. (**B**) Cells visualized with FITC-anti-SCWP (MAb EAII6G6). In the bottom cell, areas that have not yet received a deposit of S-layer allow access to the underlying SCWP and are now visualized with anti-glycosyl MAb EAII6G6 (arrows). The upper three young cells lacking S-layer are now stained uniformly with the anti-SCWP EAII6G6. The avirulent Ba684 strain is not recognized by EAII6G6 (not shown), due to the abnormal structure of its SCWP (lacking all Gal residues). The Ba684 strain does, however, express an S-layer (Figure 1). This is possible because the SCWP retains an intact pyruvylated epitope identical to that found on SCWP from *B. anthracis* Sterne, Pasteur and Ames.

of anti-EA1 (Figure 2A). These complementary patterns indicate that S-layer protein deposition blocks the access of the EAII6G6 MAb to SCWP, which underlies the S-layer deposit and anchors the S-layer components.

Purification and initial NMR analysis of the B. anthracis 684 SCWP

Chromatography of the Ba684 SCWP on a Superose SEC column yielded a peak with Kav of 0.323, corresponding to a mass of ~22,000 Da (Supplementary data, Figure S1). In comparison, the mobilities of SCWPs isolated from strains *B. anthracis* Sterne (Ba Sterne) and *B. cereus* G9241 (BcG9241) indicated masses of around 10,000 and 12,000 Da, respectively (Forsberg et al. 2011).

The ^{1}H NMR spectrum anomeric region of the Superose-purified Ba684 SCWP is compared in Figure 3 with that of the previously characterized *B. anthracis* Sterne 7702 SCWP. The Sterne SCWP consists of a HexNAc-trisaccharide backbone repeating unit, to which are attached side chain

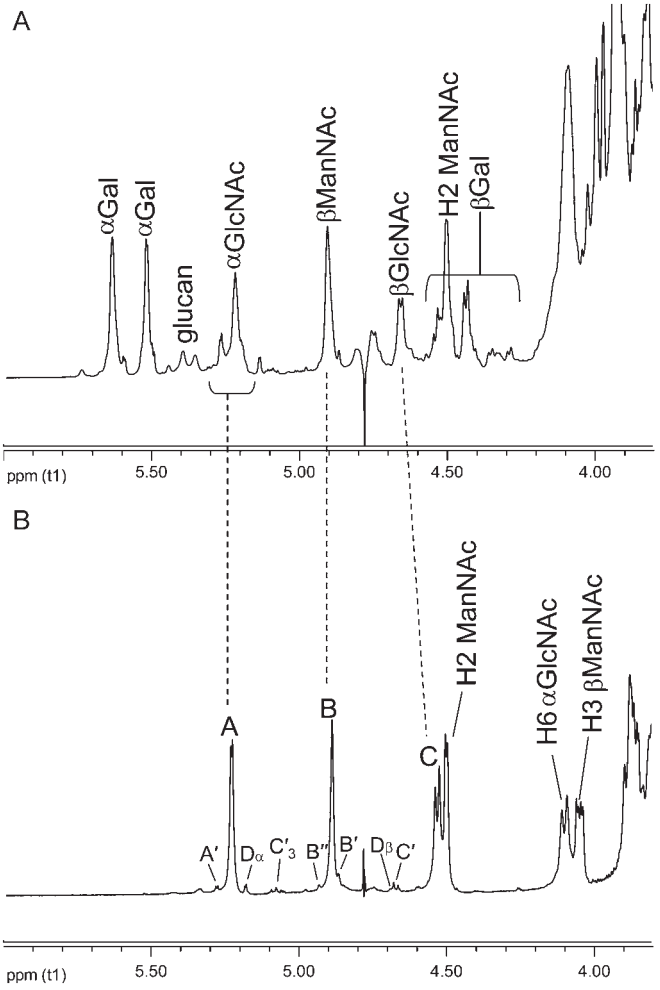

Fig. 3. Comparison of the proton NMR spectra anomeric regions for SCWPs. (**A**) *Bacillus anthracis* Sterne 7702; (**B**) Ba684. The Ba684 SCWP lacks all galactose residues; the integral ratios for the anomeric signals indicate a 1:1:1 ratio for the repeating residues **A**, **B** and **C**.

galactose residues at specific locations (Choudhury et al. 2006). Compared with the Sterne polysaccharide, the spectrum of the Ba684 SCWP was greatly simplified, yielding only three major anomeric components (**A**, **B**, **C**) in a 1:1:1 ratio. Based on their anomeric δ_H (Table I), initial inspection suggested that most or all of the galactose residues were apparently absent and that only hexosamine residues remained. These residues (**A**, **B**, **C**) designate the repeating unit residues in the SCWP. In addition, Figure 3 also shows several low-intensity anomeric signals arising from residues designated **A′**, **B′** and **C′**. These non-repeated residues carry the substoichiometric structural features, including pyruvate acetal, *O*-acetyl and free amino modifications that typify these *B. anthracis* polysaccharides. The following sections describe the structural features of the repeating unit residues (**A**, **B**, **C**) and the non-repeated, substoichiometric residues (**B′**, **B″**, **C′**, **A′** and **D**).

*NMR analysis and identification of the repeated glycosyl units (residues **A**, **B** and **C**)*

The identities of the three major spin systems (**A**, **B** and **C** in Figure 3B) were assigned from ^{1}H-^{1}H COSY (correlation spectroscopy), TOCSY (total correlation spectroscopy), NOESY (nuclear overhauser effect spectroscopy), ^{1}H–^{13}C HSQC (heteronuclear single-quantum coherence spectroscopy) and ^{1}H–^{13}C HMBC (heteronuclear multiple bond coherence spectroscopy) experiments. Scalar couplings involving anomeric resonances from TOCSY analysis, and intra-residue NOE correlations are shown in Figure 4A and B, and the ring proton–carbon correlations are shown in Figure 5A. Intra-residue and interglycosidic HMBC correlations were observed for all spin systems and are summarized in the Supplementary data, Table S1. Our results indicate that the three repeating HexNAc residues occur in an identical ratio and configuration as the three HexNAc components comprising the repeating backbone of the normal SCWPs from pathogenic *B. anthracis* and *B. cereus* (Choudhury et al. 2006; Forsberg et al. 2011). These residues are: **A**, α-Glc*p*NAc (H1 δ_H 5.23; $J_{C1,H1}$ 174.1 Hz; $J_{1,2}$ 3.3 Hz); **B**, β-Man*p*NAc (H1 δ_H 4.89; $J_{C1,H1}$ 163.6 Hz); **C**, β-Glc*p*NAc (H1 δ_H 4.53; $J_{C1,H1}$ 162.6 Hz; $J_{1,2}$ 8.2 Hz). Details of the NMR analysis describing these residues are presented in Supplementary data. Additional low-magnification COSY and NOESY spectra showing the ring proton interactions of these repeating residues (**A**, **B**, **C**) are in Supplementary data, Figure S2.

*Glycosyl sequence of repeating residues **A**, **B** and **C** as determined from inter-residue HMBC and NOE analyses*

Inter-residue NOEs (Figure 4B) and interglycosidic connectivities from ^{1}H–^{13}C HMBC analysis (Supplementary data, Figure S3) demonstrated that the Ba684 polysaccharide

Table I. 600-MHz ^{1}H and ^{13}C NMR parameters for the SCWP isolated from Ba684[a]

Residue	δ_H (ppm)							
	δ_C (ppm)[b]							
	1	2	3	4	5	6	7[c]	8[c]
Native polysaccharide								
A →6)-α-D-Glc*p*NAc-(1→	5.23	3.86	3.68	3.46	3.79	4.10/3.83	—	2.01
	99.49	54.81	71.87	70.81	72.64	69.3	175.43	23.05
B →4)-β-D-Man*p*NAc-(1→	4.89	4.50	4.05	3.66	3.56	3.89/3.80	—	2.06
	100.45	54.89	73.81	74.67	76.28	61.88	176.66	23.27
C →4)-β-D-Glc*p*NAc-(1→	4.53	3.77	3.71[d]	3.71[d]	3.51	3.88/3.73	—	2.05
	102.70	56.29	73.49	80.06	75.64	61.24	175.59	23.47
B′ (S)-Pyr-4,6)-β-D-Man*p*NAc-(1→	4.87	4.53	3.95	3.58	3.37	3.99/3.72	—	2.03
	101.08	54.70	70.16	75.12	68.01	65.32	176.f	
B″ (S)-Pyr-4,6)-β-D-Man*p*NAc-(1→	4.93	4.6	3.98	3.6	3.43	4.03/3.73	—	—
	100.53	54.77	70.48	75.09	68.01	—	—	—
C′ →4)-3-*O*-Ac-β-D-Glc*p*NAc-(1→	4.67	3.88	5.08	3.92	3.56	3.87/3.73	—	1.98
	101.93	54.64	74.99	77.03	75.64	61.24	175.58	23.21
A′ →6)-α-D-Glc*p*NH_2-(1→	5.27	2.8	3.56	3.39	3.79	4.10/3.83		
	101.30	56.15	74.12	70.68	72.6[e]	69.3[f]		
(S)-Pyruvic acid (ketal)	—	—	1.45					
	176.67	102.97	25.79					

The SCWP was purified by Superose size exclusion chromatography and subjected to NMR analysis. Additional signals: pyruvate: (C1) δ 176.67; (C2) δ 102.97; (C3) CH3 δ 25.79, CH3 δ 1.45; O-acetyl: (3-O-Ac-βGlcpNAc, residue C′) C=O δ 174.30, CH3 δ 21.72; CH3 δ 2.09. Residue D (α-reducing end): →6)-α-d-GlcpNAc, H1/C1 δ 5.18/91.74 (JC1,H1 171.8 Hz); H2/C2 δ 3.88/54.8 (H3/H4/H5/H6, 3.86/3.77/3.72/3.47, not assigned); (β-reducing end): H1/C1 δ 4.687/96.04 (JC1,H1 165.9 Hz); H2/C2 δ 3.697/54.83; (H3/H4/H5/H6, 3.87/3.83/3.71/3.51/80.08, not assigned).

[a]600 MHz spectra measured at 25°C in D_2O relative to internal DSS (δ_H 0.00 ppm). $J_{C1,H1}$ and $J_{H1,H2}$ values for each glycosyl residue are given in the *Results* section.

[b]Carbon δ_C obtained from ^{1}H-detected HSQC spectra; carbonyl δ_C from the ^{1}H–^{13}C HMBC spectra.

[c]Positions 7 and 8 refer to *N*-acetyl moiety.

[d]δ H3 = 3.708; δ H4 = 3.714; carbon assignments at positions 3 and 4 were deduced from intra residue ^{1}H–^{13}C HMBC correlations, consistent with ^{1}H–^{13}C HSQC values, as described in *Results* and Supplementary Data Table S1.

[e]The carbon shift could not be assigned accurately since it is obscured by H5/C5 from the repeated α-GlcNAc (residue **A**).

[f]The carbon shift could not be assigned accurately since it is obscured by H6/C6 from the repeated α-GlcNAc (residue **A**).

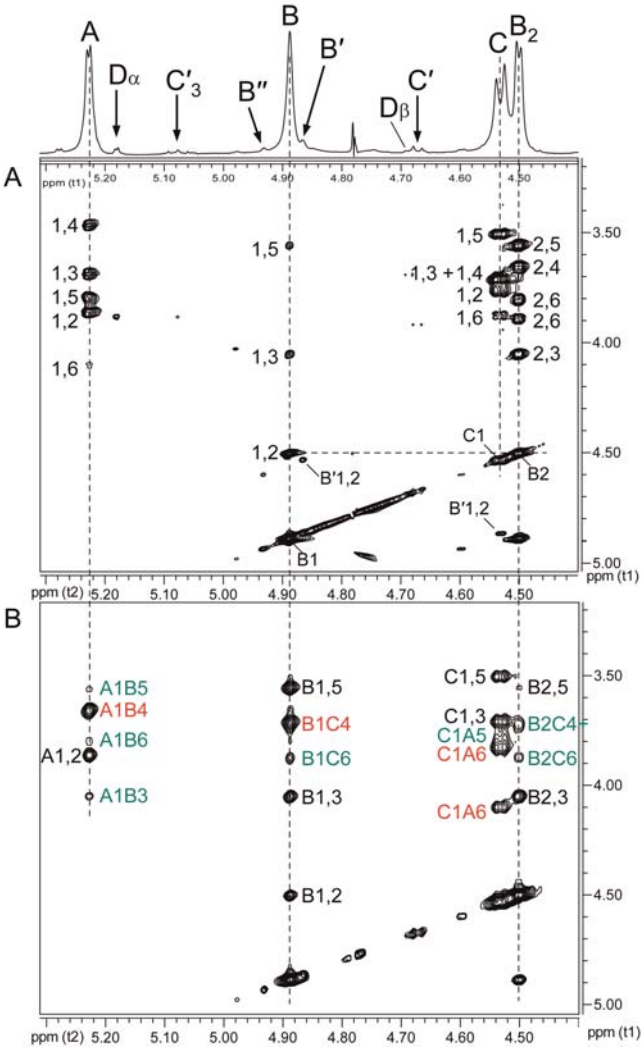

Fig. 4. Partial ^{1}H–^{1}H TOCSY and ^{1}H–^{1}H NOESY spectra of the Ba684 SCWP. (**A**) TOCSY and (**B**) NOESY. These spectra, at low magnification, allow clear resolution of the anomeric region connectivities for the repeating residues only (residues **A**, **B** and **C**); connectivities for substoichiometric, non-repeating residues of low intensity are not visible.

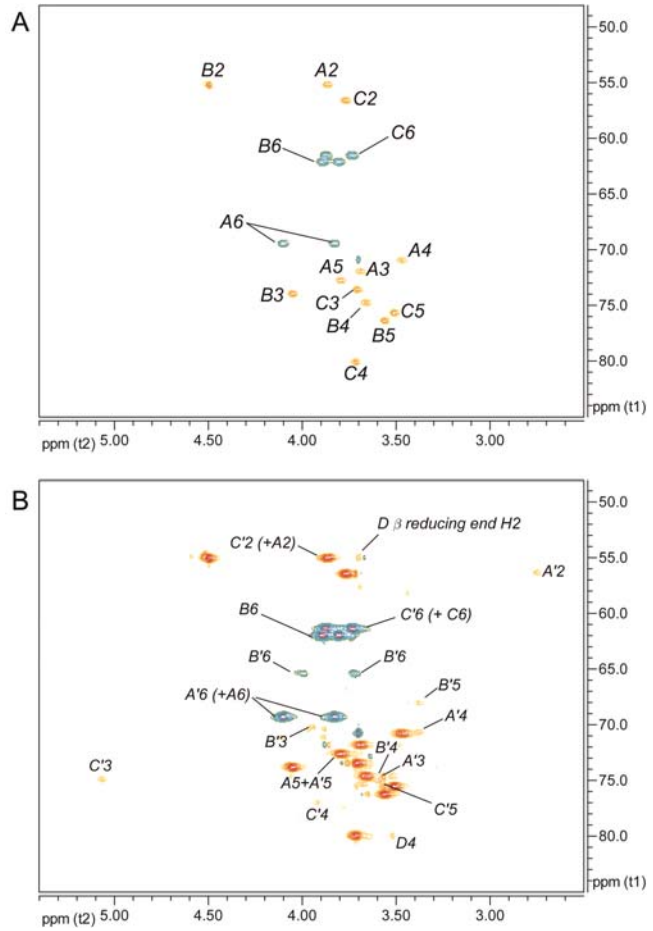

Fig. 5. Partial ^{1}H–^{13}C HSQC spectra of the Ba684 SCWP. (**A**) Ring proton region at low intensity, showing signals arising from the repeating unit residues; (**B**) the same region at very high intensity, allowing visualization of weak signals arising from substoichiometric structurally modified residues. Signals of positive polarity (e.g. A5, B4, etc.) arise from (C-H), and signals of negative polarity arise from (CH_2) moieties, e.g. C6 of hexopyranose.

consisted of a repeating trisaccharide unit having the structure →4)Bβ(1 → 4)Cβ(1 → 6)Aα(1→. These results indicated the repeating trisaccharide sequence →4)-β-D-Man*p*NAc-(1 → 4)-β-D-Glc*p*NAc-(1 → 6)-α-D-Glc*p*NAc-(1→, identical in all respects to the glycosyl backbones shared by all *B. anthracis* strains (Choudhury et al. 2006) and pathogenic *B. cereus* strains (Forsberg et al. 2011) examined. Details of the NMR parameters defining this glycosyl sequence are included in the Supplementary data.

*Localization of pyruvate acetal, O-acetate and other substoichiometric modifications on residues **B′**, **C′** and **A′** of the Ba684 SCWP*

The various NMR spectra from the Ba684 SCWP, and all previously examined SCWPs from strains *B. anthracis* Sterne, Pasteur and Ames and pathogenic *B. cereus* (Choudhury et al. 2006; Forsberg et al. 2011), consistently show weak, low-intensity signals that occur at a stoichiometry far below that of the repeated glycosyl residues. Although some of these signals inevitably arise from contaminants, many, as shown here, arise from non-repeated structural features of the SCWP, i.e. modifications occurring on only one or a few repeating units at specific locations. These "reporter" signals are virtually superimposable among the various strains; they are particularly evident during ^{1}H–^{13}C HSQC analysis and fall into three main categories; (i) signals associated with pyruvylation; (ii) signals arising from substoichiometric *O*-acetylation and (iii) signals associated with amino-group modification of 2-aminohexose residues. Since the Ba684 SCWP lacks, all of the repeated galactose residues that are normally present in the fully galactosylated SCWPs from pathogenic strains of *B. anthracis* and *B. cereus*, the NMR spectra of the Ba684 SCWP are greatly simplified. This facilitates detection and assignment of the complete spin systems associated with the substoichiometric modifications, since many of these signals are otherwise masked by galactose signals present in the pathogenic and typical strain spectra.

Residue ***B′***. In the case of pyruvate, Ba684 SCWP contains a small (substoichiometric) methyl group resonance (δ_H 1.46, Supplementary data, Figure S4) and HMBC connectivities identify the associated spin system as that of pyruvate acetal (Table I); in particular, the C2 shift (δ_C 102.97) is indicative of a six-member cyclic ketal ring (Garegg et al. 1980; Gorin et al. 1982; Mesnage et al. 2000), indicating that pyruvate in the sample is indeed linked to some type of carrier. The Ba684 SCWP and all *B. anthracis* and pathogenic *B. cereus* SCWPs examined to date (Choudhury et al. 2006; Forsberg et al. 2011) contain this identical spin system, and integration of the ^{1}H spectra from all of these samples consistently indicates a ratio of ∼10:1 for anomeric resonance:pyruvate methyl group (where "anomeric resonance" is the area of H1 from any repeated glycosyl residue (**A**, **B** or **C**), and "pyruvate methyl group" refers to the combined area of all three pyruvate protons). Based on the masses of the SCWP (Forsberg et al. 2011), this is equivalent to one residue of pyruvate per every 10 repeating units, or essentially one pyruvate per typical SCWP molecule in the case of these pathogenic *B. anthracis* and *B. cereus* polysaccharides. To investigate possible sites of pyruvylation, an initial clue was presented by re-examination of the ^{1}H–^{13}C HSQC spectra for substoichiometric signals. For the Ba684 SCWP, magnification of the signal intensity ("*z*"-axis, Figure 5B) revealed a set of connectivities with a carbon shift intermediate between that of unsubstituted and glycosylated primary hydroxyls (i.e. C6 position), δ_H 3.99/3.72 and δ_C 65.32. These signals displayed negative polarity (indicative of methylene hydrogens, –CH_2OR) and were of interest since their overall intensity was well below (∼10-fold) that of the repeating residue signals (compare Figure 5A) consistent with the substoichiometric attachment of a single residue of pyruvate. In fact, the δ_C of these putative H6/C6 signals appeared consistent with published shifts for pyruvate acetalation at O6 (Ziegler et al. 1993; Petersen et al. 2008). Assuming validity as C6/H6 signals, and tracing scalar coupling back to H1 using COSY and TOCSY, a weak spin system was identified and readily defined as a 2-aminohexopyranose. In fact, all proton positions of this residue could be unambiguously assigned from COSY analysis alone (Figure 6), with strong coupling from H6 through H3, and unique δ_H shifts distinct from those of the repeated residues (Table I). The $J_{C1,H1}$ (163.8 Hz) and NOEs between H1/H3 (δ_H 4.87/3.95), H1/H5 (δ_H 4.87/3.37) and H3/H5 indicated a $^4C_1$ β-pyranose. This residue (designated **B′**) was assigned the *manno*-configuration based on the downfield resonance at H2 (δ_H 4.53), unresolved $J_{1,2}$ (<1 Hz) for a β-pyranose, and a strong NOE between H1/H2, factors which would not typify a β-*gluco*-pyranose. In addition, TOCSY analysis indicated that scalar coupling from H1 was weak beyond H2, with strong coupling commencing at H2 through H6 (Figure 4A and Supplementary data, Figure S5). Carbon shifts at C6, C5 and C4 are also consistent with literature values for pyruvate acetalation at O6 and O4 (Ziegler et al. 1993; Petersen et al. 2008), including the unusual upfield shift at C5, presumably reflecting shielding due to the "γ"-effect from substitution with a bulky group. Also noteworthy, the C3 shift (δ_C 70.16) indicates that this residue is likely not substituted at O3 (Lipkind et al. 1988; Agrawal, 1992), and therefore, **B′** is a terminal non-reducing end of the SCWP.

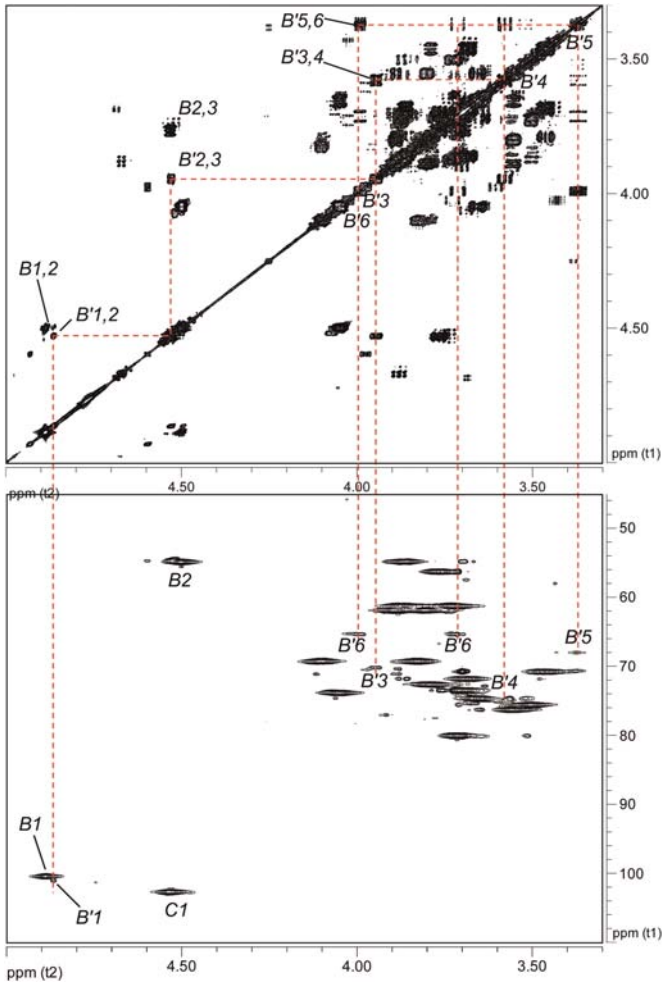

Fig. 6. Partial ^{1}H–^{1}H COSY and ^{1}H–^{13}C HSQC spectra of the Ba684 SCWP defining the terminal pyruvylated-ManNAc (residue **B′**). Top panel, COSY; bottom panel, HSQC. The spectra, displayed at high magnification, allow the visualization of the weak signals arising from the **B′** spin system. This residue occurs at only one location, the terminal non-reducing end of the SCWP.

A candidate residue now defined, consistent with a 4,6-pyruvylated β-Man*p*NAc, direct evidence was sought for pyruvate attachment. This was provided by a 3-bond HMBC correlation between the pyruvate acetal carbon (δ_C 102.97) and a proton at δ_H 3.99, one of the H6 protons of **B′** (Figure 7). With the position of acetalation and the glycose configuration established, complete assignment of pyruvate configuration was possible. The δ_H/δ_C at pyruvate H3/C3 and at C2 (Table I) are exactly consistent with an equatorial orientation of the pyruvate methyl group (Garegg et al. 1980), yielding the (S)-configuration for this moiety. *N*-Acetylation of residue **B′** at the 2-position was supported by a weak HMBC between H2 (δ 4.53) and a carbonyl carbon (δ_C 175.32) (Supplementary data, Figure S6). With the location of the (S)-4,6-*O*-(1-carboxyethylidene)-β-Man*p*NAc residue as a terminal, non-reducing end established, its linkage to the remainder of the SCWP was elucidated by interglycosidic HMBC and NOE connectivities.

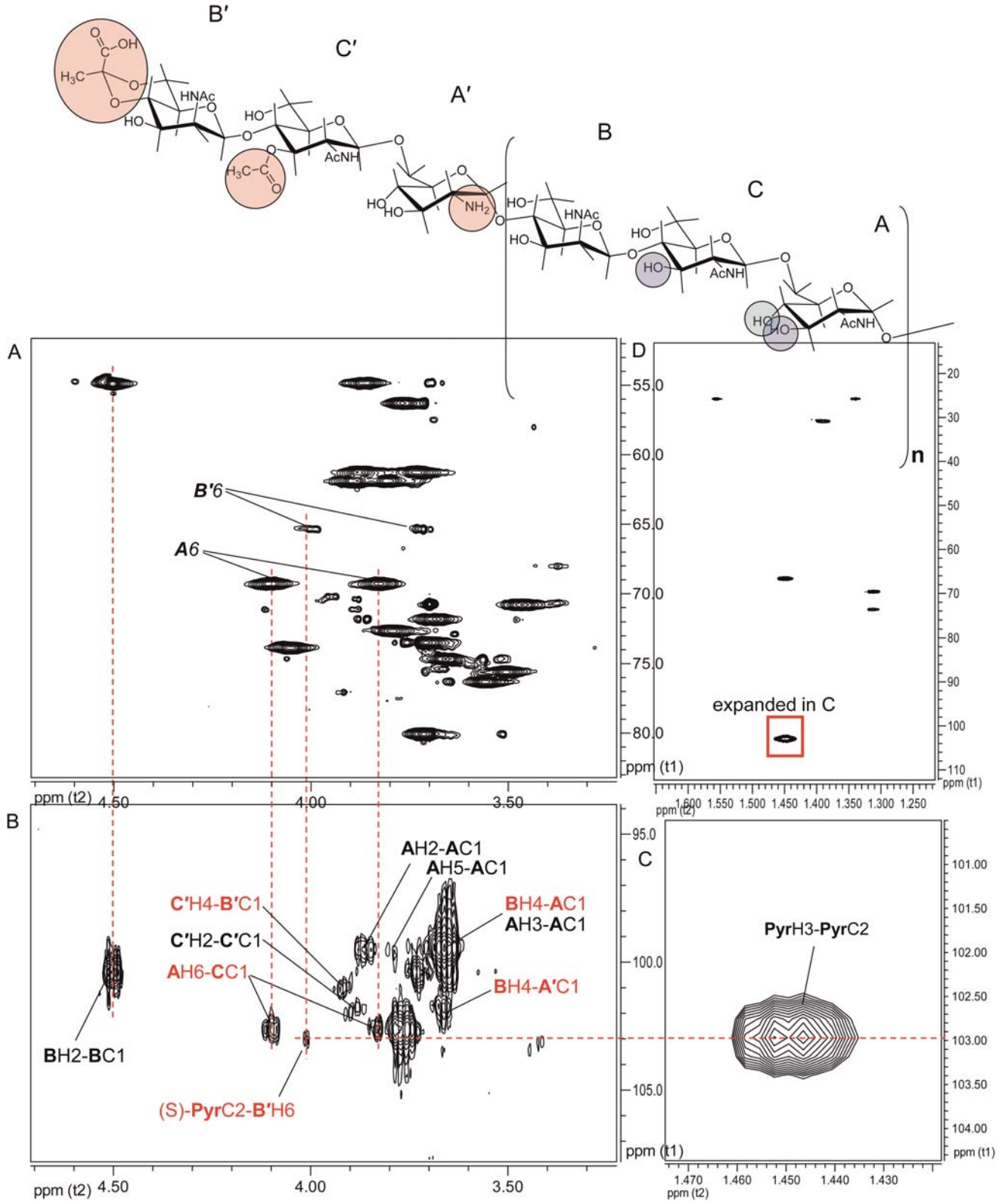

Fig. 7. Partial 600-MHz NMR spectra indicating the linkage of pyruvate to the terminal ManNAc residue in Ba684 SCWP. (**A**) $^{1}H–^{13}C$ HSQC; (**B**) $^{1}H–^{13}C$ HMBC; (**C** and **D**) HMBC spectra of the pyruvate spin system. The spectra are shown at high intensity to allow the visualization of this structural modification, which occurs at one location in the SCWP. Favorable bond geometry and magnetic environment yield coupling between **Pyr**C2 and one of the **B′**H6 protons. Circled moieties on **B′**, **C′** and **A′** highlight the substoichiometric structural modifications, and circled positions on **B**, **C** and **A** indicate the position of galactosylation in the *B. anthracis* Sterne, Pasteur and Ames SCWPs.

Residue **C′**. Another previously unexplained, substoichiometric signal present in the HSQC spectra of all SCWPs from pathogenic Ba and Bc strains, and the Ba684 SCWP, is a weak connectivity at δ_H/δ_C 5.08/74.99 (subsequently assigned H3/C3 of residue **C′**) consistent with a de-shielded methine proton attached to carbon bearing an *O*-acyl group (Figure 8). Commencing with the equivalent weak proton signal in the COSY, and referring to TOCSY couplings, an entire spin system could be delineated consistent with a 3-*O*-acetyl-2-aminohexopyranose, the analysis again facilitated at all positions by the absence of interference from galactose residues. This residue (**C′**) was evident in the COSY and HSQC spectra (Supplementary data, Figure S7) with well-resolved scalar couplings between H3/H4 (δ 5.08/3.92), H3/H2 (δ 5.08/3.88), H2/H1 (δ 3.88/4.67), H4/H5 (δ 3.92/3.56), H5/H6a (δ 3.56/3.87) and H5/H6b (δ 3.56/3.73) (Supplementary data, Figure S8). TOCSY connectivities were evident for all protons except H6a (obscured by H2, Supplementary data, Figure S9). The $J_{C1,H1}$ (163.3 Hz) and $J_{1,2}$ (8.9 Hz) indicated the β-anomeric configuration for a hexopyranose, and intra-residue NOEs between H1/H3, H1/H5, H3/H5 (Supplementary data, Figure S9) and H2/H4 (not shown) were consistent with a $^4C_1$ chair and β-*gluco*-pyranose configuration. An NOE was not observed between H1/H2, and δ_H H2 was typical of Glc*p*NAc not Man*p*NAc (Agrawal 1992), additional factors pointing to identification as a 3-*O*-acetyl-β-Glc*p*NAc (**C′**). The location of the acetyl group at O3 was substantiated by HMBC connectivities between H3 and a carbonyl carbon (δ_C 174.30, Supplementary data, Figures S10 and S11) and between this carbonyl carbon and methyl protons (δ_H 2.09). Other intra-residue HMBC connectivities confirmed carbon assignments at each position (Supplementary data, Table S1). The δ_C assignments suggested that **C′** is glycosidically substituted at C4, downfield shift δ 77.03 (Lipkind et al. 1988; Agrawal 1992). The magnitude of the C4 shift is 3.03 ppm upfield from δ C4 of the repeating, non *O*-acetylated β-GlcNAc (compare residue **C**, Table I), consistent with shielding due to *O*-acetylation at O3 ("β-effect") (Jansson et al. 1987). An "α-effect" (deshielding, magnitude 1.5 ppm) at position 3 was also observed relative to the non *O*-acetylated residue **C**. As shown below, glycosidic substitution at O4 of **C′** was confirmed by inter-residue connectivities.

Residue ***A′***. A final set of minor, "reporter" signals (subsequently assigned to residue **A′**) is present in the HSQC spectrum of the Ba684 SCWP, and analogous signals were again identified in the spectra of all previously examined *B. anthracis* and pathogenic *B. cereus* SCWPs examined to date (Figure 9). These unique signals at δ_H/δ_C 2.80/54.81 were found to drift slightly (e.g. δ_H 2.80 → 2.74; Supplementary data, Figure S12) during sample manipulation (concentration during transfer to a new NMR tube, pH and ionic strength-induced changes), suggesting the presence of a free amino group at the carbon bearing the δ 2.80 proton. This signal "drift" at H2 and adjacent positions was an assist while assigning configuration to this residue. The TOCSY and COSY spectra revealed strong couplings involving the δ 2.80 proton with five other protons (although all signal intensities were of less abundance compared with the repeated-glycosyl residues), indicating that the δ 2.80 proton is part of a coupled system (ruling out the possibility that δ_H 2.80 proton originated from an *N*-methyl group). Together, the coupled protons and their assigned carbons were assigned positions H1 through H6 (residue **A′**, Table I), which along with the $J_{C1,H1}$ (171.1 Hz) allowed assignment as an α-2-aminohexopyranose. Intraresidue NOEs between H2/H4 and H3/H5 (not shown) were consistent

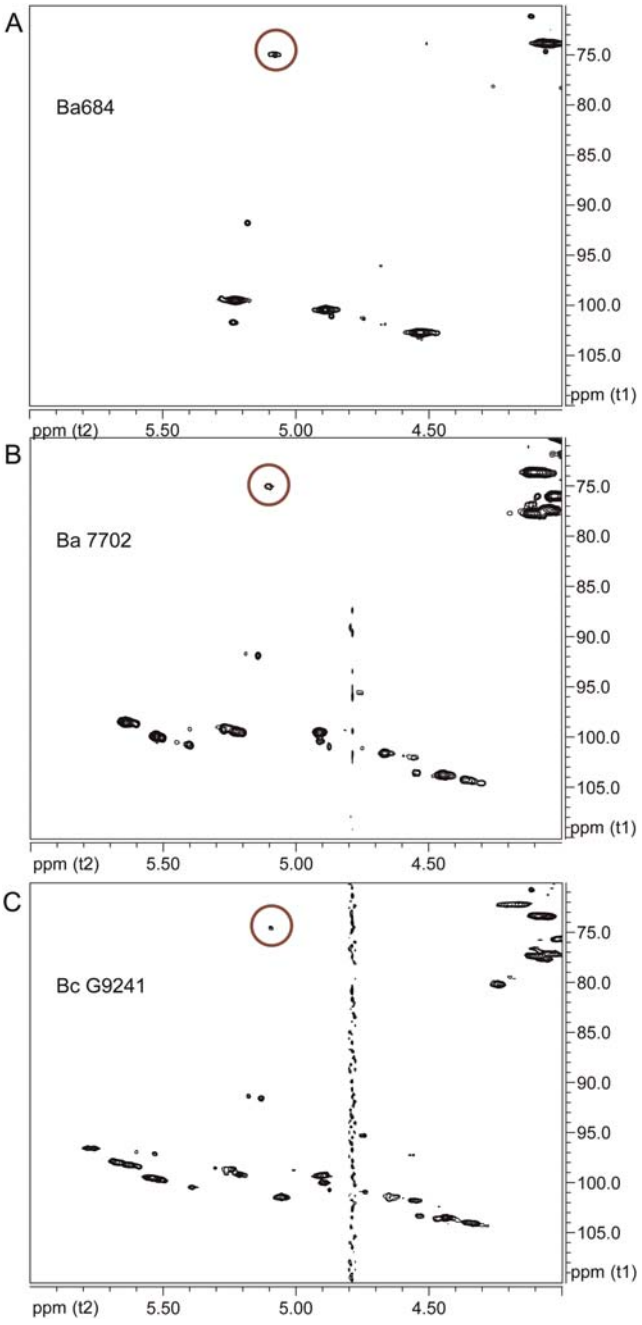

Fig. 8. Comparison of ^1H–^{13}C HSQC spectra anomeric regions of SCWPs showing certain substoichiometric structural modifications (residue **C′**) common to all of these strains. (**A**) *Bacillus anthracis* CDC 684; (**B**) *B. anthracis* Sterne 7702; (**C**) *B. cereus* G9241. The weak signal arising from H3/C3 of the 3-*O*-acetylated β-GlcNAc (residue **C′**) is circled.

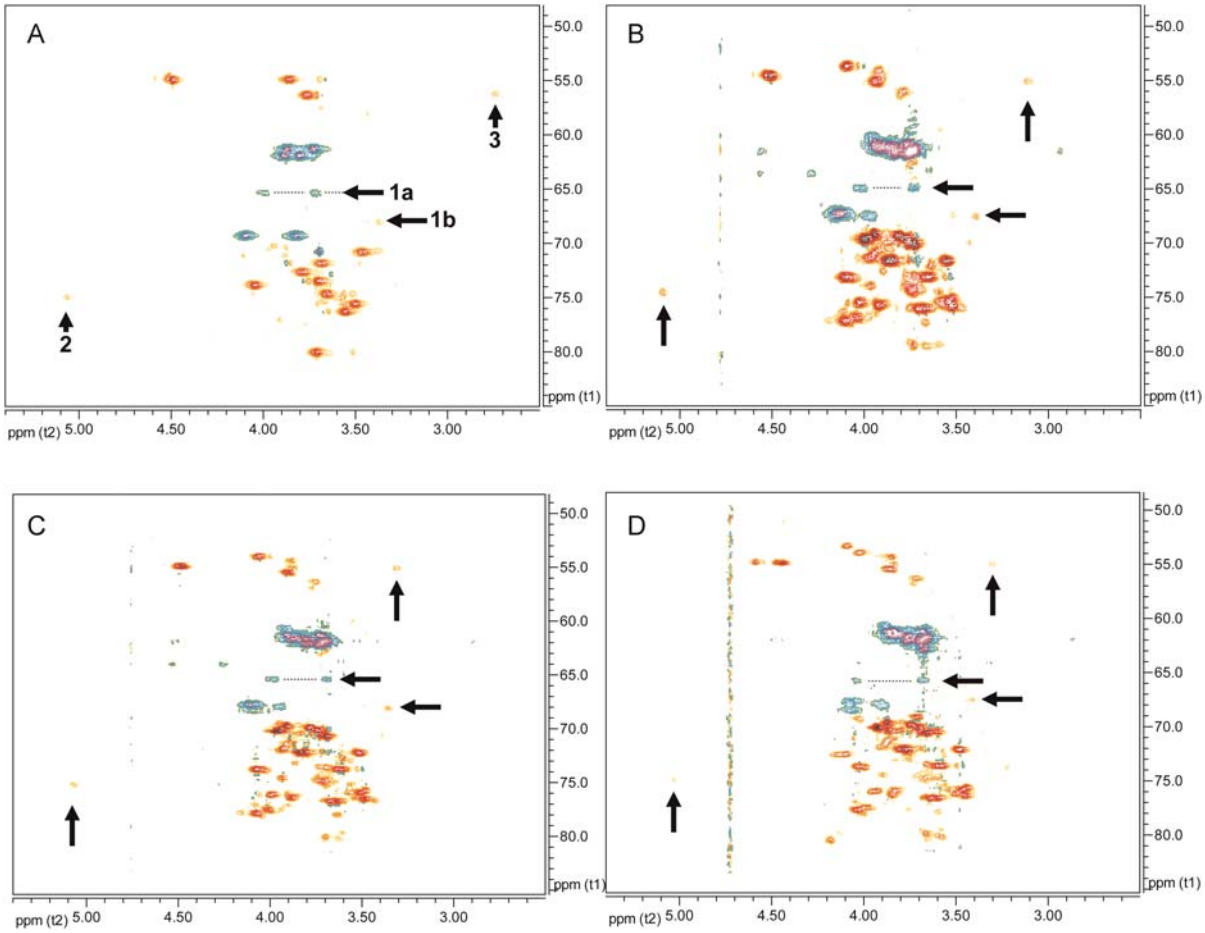

Fig. 9. Comparison of ^{1}H–^{13}C HSQC NMR spectra of SCWPs showing the reporter signals arising from pyruvylated, *O*-acetylated and related structurally modified residues common to *B. anthracis* and certain *B. cereus* strains examined. (**A**) *Bacillus anthracis* CDC 684; (**B**) *B. anthracis* Sterne 7702; (**C**) *B. anthracis* Sterne 34F_2; (**D**) *B. cereus* G9241. The "reporter signals" arise from the non-repeated, structurally modified glycosyl residues that are located exclusively at the non-reducing end of the molecule. Arrows: (1) signals diagnostic of pyruvylation; 1a arises from H6/C6 of residue **B′**, and 1b arises from H5/C5 of **B′**; (2) signal indicative of 3-*O*-acetylation, from H3/C3 of residue **C′**; (3) signal indicative of free 2-amino group, H2/C2 of residue **A′**.

with a $^{4}C_1$ chair conformation for a α-Glc*p*NH_2 residue, lacking *N*-acetylation.

*Glycosidic sequence and location of residues **B′**, **C′** and **A′** on Ba684 SCWP*

Interglycosidic HMBC connectivities were readily detected between all three of these non-repeated residues, yielding the sequence **B′**β(1 → 4)**C′**β(1 → 6)**A′**α(1→, and also to the main polysaccharide chain, from **A′** to repeating residue **B** (spectra shown in Supplementary data Figures S10 and S11), revealing the non-repeating terminal sequence shown in Figure 7, in which all three residues of the non-reducing terminal repeating unit are modified. These interglycosidic connectivities (Supplementary data, Table S1) could be rather easily distinguished from those of the repeating-residues, due to their unique chemical shifts and stoichiometry. Residue **B′** exhibited two interglycosidic HMBC couplings to **C′**, from **B′**H1-**C′**C4 and from **B′**C1-**C′**H4, supported by an NOE between **B′**1/**C′**4 (δ 4.87/3.92, Supplementary data, Figure S5). Residue **C′** yielded a single interglycosidic HMBC coupling to **A′**, between **C′**H1-**A′**C6, supported by an NOE between **C′**1/**A′**6 (δ 4.67/4.10, Supplementary data, Figure S9). Residue **A′** also displayed interglycosidic HMBC coupling to a normal (repeating) residue B, between **A′**C1-BH4 (Figure 7), in addition to an NOE between **A′**1/B4 (δ 5.27/3.66).

*Demonstration of the terminal non-repeating sequence (**B′**-**C′**-**A′**) in SCWPs from pathogenic and typical B. anthracis and B. cereus SCWPs*

Re-inspection of the HSQC spectra from all previously examined normal strain-SCWPs (derived from pathogenic *B. anthracis* and *B. cereus*) revealed that all spectra show virtually identical substoichiometric "reporter" signals indicating the presence of structural modifications, identical or very similar to those detected in the Ba684 non-galactosylated polysaccharide. Representative HSQC spectra from *B. anthracis* Sterne 34F_2, 7702 and *B. cereus* G9241 are compared with Ba684 SCWP in Figure 9. Reporter signals: (1) residue **B′**—primary hydroxylated carbon bearing methylene hydrogens (representing C6 of glycose residues, R-CH_2OR), and resonating downfield with a δ_C intermediate between that of unsubstituted and glycosidically substituted primary hydroxyl

group); at high signal intensity, all spectra showed weak signals of negative polarity, virtually superimposable with the H6/C6 signals attributed to a 4,6-pyruvylated β-Man*p*NAc in the Ba684 SCWP, Figure 9. The remarkably identical δ_H/δ_C shifts of this signal set among the spectra indicate a similar or identical magnetic environment of the pyruvate-glycose moiety, suggesting all may occupy a terminal, non-reducing location on each polysaccharide. In these fully galactosylated SCWPs, the remaining ring positions of the pyruvylated-glycose were not readily assignable due to masking by signals arising from α/β-Gal substituents; (2) residue **C′** – methine hydrogen attached to a secondary carbon bearing an *O*-acetyl group; also of weak intensity, this reporter group consistently stands out in the HSQC spectra of all SCWP examined to date having nearly superimposable δ_H/δ_C from strain to strain, Figures 8 and 9. This indicates that the fully galactosylated, normal strain SCWPs contain a single *O*-acetylated glycose residue, similar or identical to the penultimate 3-*O*-Ac-β-Glc*p*NAc residue in Ba684 SCWP, and the weak intensity indicates it is non-repeated; (3) residue **A′**– methine hydrogen attached to a carbon bearing a free amino group (non *N*-acetylated). In all pathogenic strain SCWPs examined to date, the δ_H of this moiety ranges from about δ_H 2.7–3.1 ppm and the δ_C is typically 53–56 ppm (Figure 9). These results indicate the substoichiometric occurrence of a glycose-linked free amino group, analogous to the non-repeated α-Glc*p*NH_2 residue found in Ba684 SCWP.

The presence of these unique reporter signals indicates the substoichiometric presence of residues equivalent to **A′**, **B′** and **C′** in all of these SCWPs, even though the complete spin systems could not be entirely defined due to masking by galactosylation. However, interglycosidic connectivities, analogous to those observed in Ba684, were also detected at substoichiometric levels in the HMBC and NOE spectra from all pathogenic strains of *B. anthracis* and *B. cereus* SCWP. These long range connectivities suggest that the non-repeating residues are linked in the same sequence and at identical location (terminal, non-reducing end) to the remainder of the polysaccharide as in Ba684 SCWP. Representative of the pathogenic *B. anthracis* SCWP spectra, and virtually identical with the Ba684 spectra, a three-bond HMBC connectivity between pyruvate C2 and the analogous substoichiometric **B′** H6 signal is shown for *B. anthracis* Sterne, Supplementary data, Figure S13.

*Other substoichiometric glycosyl residues (**B″** and Dα/β)*

Two other residues, of similar weak stoichiometry are visible in the ^{1}H spectrum anomeric region and were identified (Supplementary data Figures S5, S7, S9, S11). Residue **B″** (Table I, H1 δ_H 4.93) is a subset of pyruvylated residue **B′**. This residue is a 4,6-pyruvylated terminal Man*p*NAc that is linked to a normal, (i.e. non 3-*O*-acetylated) Glc*p*NAc, indicating that a subset of the polysaccharides terminate in pyruvate-ManNAc only, and lack the *O*-acetyl modification on GlcNAc. Acetylation at O3 of the penultimate GlcNAc residue is apparently sufficient to alter the magnetic environment of the terminal ManNAc residue slightly at positions 1 thru 6 to various extents. Glycosidic linkage between **B″** and (non-*O*-acetylated) residue **C** was evidenced by an inter-residue NOE between **B″**1/C4 (δ 4.93/3.706, Supplementary data, Figure S5; compare to δ 4.89/3.714 for the repeating B1/C4) and by the interglycosidic HMBC crosspeak **B″** H1-CC4 (δ 4.93–78.63, Supplementary data, Figure S11). There was no compelling evidence for the presence of any terminal ManNAc residues lacking pyruvate, indicating that most or all of the SCWP terminate in a pyruvylated residue.

An additional residue, present at low abundance (Supplementary data, Figures S7, S9, S10, S11) was assigned as the free reducing end and identified as Glc*p*NAc (α-anomer major form; Dα/Dβ, δ_{H1} α 5.18; δ_{H1} β 4.67). The complete spin system could not be assigned, however, beyond H3. Assignment as a Glc*p*NAc is based solely on C1/H1 and C2/H2 shifts (Table I) and coupling constants (α, $J_{C1,H1}$ 171.8 Hz; β, $J_{C1,H1}$ 165.9 Hz). The presence of a free reducing end glycose is also consistent with ^{31}P direct observed NMR, which indicated an absence of phosphate ester signals of any type in this preparation. In this study, the reducing end glycosyl sequence was not examined beyond this point, and any glycosyl sequence differences, if they exist, between the reducing end region and the repeating unit residues were not immediately evident.

Discussion

The secondary wall polysaccharide of Ba684 was of interest for several reasons, (1) relatively little information exists on the structures of *B. anthracis* and related *B. cereus* SCWPs, limiting our understanding of their role in cell viability, wall assembly and virulence; (2) this particular strain is one of the very few known naturally occurring *B. anthracis* strains which fail to react with monoclonal antibody EAII6G6 (Ezzell et al. 1990; De et al. 2002), which is used diagnostically to identify *B. anthracis* strains and is known to recognize a wall polysaccharide epitope specific for and expressed by *B. anthracis* strains, thus suggesting that the SCWP elaborated by CDC 684 could be either defective or absent; (3) the Ba684 strain is avirulent, even though it carries both virulence plasmids (pXO1 and pX02), and resides within the same phylogenetic lineage as the highly pathogenic *B. anthracis* Vollum (Okinaka et al. 2011). The Ba684 chromosome differs from that of Vollum by only 51 unique SNPs (Okinaka et al. 2011), however a biochemical basis for the lack of pathogenicity of this organism has not been formulated; (4) of particular interest, although the results were not anticipated, analysis of the CDC 684 SCWP has revealed several key structural modifications, that we now know are shared by all previously examined pathogenic *B. anthracis* strains, allowing localization and characterization of a conserved pyruvylated epitope on these *B. anthracis* SCWPs. These structural modifications occur at the substoichiometric level (i.e. they occur only at specific locations and not on every repeating unit) of the Ba684 SCWP, and they appear to occur in identical manner and location on the SCWPs of all *B. anthracis* strains (Pasteur, Ames and Sterne 34F_2 and 7702) examined to date (Choudhury et al. 2006), as well as a number of previously examined pathogenic *B. cereus*, strains G9241 and 03BB87 (Forsberg et al. 2011). These structural modifications consist of three contiguous, structurally modified glycosyl residues located

exclusively at the distal (non-reducing) end of each SCWP, and are likely to constitute an epitope mediating SLH-domain protein adhesion and deposition.

Our results show that Ba684 synthesizes a SCWP, however, although the backbone is fully polymerized and has a sequence identical to that found in pathogenic *B. anthracis*, the SCWP is devoid of all galactose side residues, a significant difference from the highly galactosylated SCWPs of pathogenic strains. This raises questions about SCWP biosynthesis, suggesting that backbone polymerization and side residue attachment can occur independently for this class of polysaccharide. This could help account for the extensive heterogeneity in side residue attachment observed in the SCWPs from strains of *B. anthracis* (Ames, Sterne, Pasteur) and *B. cereus* examined to date (Choudhury et al. 2006; Leoff et al. 2008; Candela et al. 2011; Forsberg et al. 2011). These and other examined *Bacillaceae* (Schäffer and Messner, 2005; Petersen et al. 2008) indicate a noticeable lack of adherence to any strict requirement for repeating unit uniformity in this class of *Bacillus* PS.

Our immunochemical analyses indicate that Ba684 cells, like all non-encapsulated *B. anthracis* (Fouet 2009) synthesize and express an S-layer (Figure 1), based on reactivity with the anti-EA1 polyclonal antiserum (Farchaus et al. 1995). These results indicate that Ba684 must express a pyruvylated cell surface epitope (the recognition anchor for SLH-domain proteins such as EA1) and are consistent with our structural observation that the Ba684 SCWP carries a pyruvate residue, even though it lacks all of the galactose side chains. Thus, the absence of all α/β-Gal side chains in this SCWP does not appear to significantly interfere with S-layer protein deposition. In contrast, our finding that the Ba684 SCWP lacks all Gal side residues accounts for the failure of this strain to bind the anti-Gal-HexNAc MAb EAII6G6, used diagnostically to detect pathogenic *B. anthracis* (Ezzell et al. 1990). Mapping of the complete EAII6G6 epitope carried on the highly galactosylated SCWPs from pathogenic *B. anthracis* is in progress (N. Kamal et al. in preparation).

Using the biosynthesis of wall teichoic acids (WTA) as a model, (Schäffer and Messner 2005; Bhavsar and Brown 2006; Swoboda et al. 2010) the attachment of the Gal side residues to the *B. anthracis* SCWP backbone could involve a TagE homologue (or other glycosyl transferase), possibly disrupted in Ba684 due to one or more of the 51 SNPs identified in this strain (Okinaka et al. 2011). In Ba684, the disruption of Gal transferase activities is not lethal, but the resulting structural defect (absence of all Gal side residues) would likely result in altered conformational dynamics of the polysaccharide, possibly resulting in defective wall assembly and ultimately contributing to the altered growth kinetics observed for this strain (Okinaka et al. 2011). In this regard, it is noteworthy that SLH-domain proteins are not restricted to the S-layer glycoproteins, and in *B. anthracis* also include at least 18 other proteins, three of which are coded on the virulence plasmids and over 15 are chromosomal in origin (Okinaka et al. 1999; Mesnage et al. 2000; Kern and Schneewind 2008). Several of these proteins reportedly have similarity to PG hydrolyases and may play a role in PG remodeling, wall turnover and function and cell division. Although S-layer synthesis does occur in Ba684, as indicated by EA1 deposition (Figure 1B), the adhesion of other macromolecules, such as endogenous autolysins essential for PG remodeling or phage endolysins, that may require both a pyruvylated and fully galactosylated–HexNAc epitope, would likely be altered or diminished in the Ba684 strain (Mesnage et al. 2000; Swoboda et al. 2010). A further consideration is that the unexplained avirulence of Ba684 could be due, in part, to its slower growth rate, allowing increased pressure from the host immune system. Thus, a possible connection between SCWP structure and virulence is noted.

The SCWPs from *B. anthracis* (strains Ames, Pasteur and Sterne) and closely related pathogenic *B. cereus* (strains G9241, 03BB87 and 03BB102) are small polysaccharides ranging in size from 10,000 to 12,000 Da (Mesnage et al. 2000; Forsberg et al. 2011). All of these SCWP are of relatively uniform size for a polysaccharide, as estimated chromatographically (Ekwunife et al. 1991; Mesnage et al. 2000; Forsberg et al. 2011), and each SCWP typically consists of 10 repeating units on average (Forsberg et al. 2011); thus the entire backbone of each SCWP is typically 30 HexNAc residues in length. In contrast, our present results indicate that chain length polymerization appears highly altered in the Ba684 SCWP. The structural analysis and estimated size of 22,000 Da indicates a linear non-galactosylated chain of approximately 100 HexNAc residues. Possibly, the inability to attach Gal side residues to the growing HexNAc polymer interferes with the normal mechanisms governing chain length (e.g. tethering of growing polymer to enzyme).

As shown in this report, the HF-released SCWPs of *B. anthracis*/*B. cereus*/Ba684 appear unique in that a pyruvate residue occurs at only one location, the terminal β-ManNAc residue located at the distal non-reducing end, opposite the end linked to PG. Such a terminal location could promote involvement in recognition events such as SLH-domain adhesions. In the normal strain highly galactosylated SCWPs, the linkage positions of Gal and HexNAc would actually preclude pyruvate cyclic ketal formation at any of the interior HexNAc residues. The finding, that chains terminate in pyruvylated-ManNAc, also establishes the correct "frame shift" of the glycosyl backbone in these SCWPs. Pyruvylation at ManNAc seems to be a feature of many *Bacillus* polysaccharides (Kojima et al. 1988; Schäffer et al. 2000; Schäffer and Messner, 2005; Petersen et al. 2008) and may be a further characteristic of an ancestral origin of this epitope. The SCWP from *Geobacillus stearothermophilus* PV72/p2, also released from PG by HF, contained pyruvate substitution on every repeating unit and in 4,6-linkage to ManNAc (Petersen et al. 2008).

Other, previously unknown features of this putative SLH-recognized epitope in *B. anthracis* SCWP include the presence of a single *O*-acetyl group at O3 of the penultimate β-GlcNAc residue (adjacent to the pyruvylated-ManNAc) and the presence of a free 2-amino group on a α-GlcNH_2 residue. All of these modifications, localized at the nonreducing end, are likely to be key directive elements in any epitope or binding site, providing a potential source of hydrogen-

bonding, charge/zwitterionic interaction and other noncovalent interaction. Recently, *O*-acetylation of PG was proposed as a requirement for SLH-protein anchoring on the *B. anthracis* surface (Laaberki et al. 2011), however the role of SCWP or a requirement for *O*-acetylation of SCWP in adhesion was not examined in that study. This substoichiometric 3-*O*-acetylated-β-GlcNAc modification of SCWP described here, located immediately adjacent to the pyruvylated ManNAc, suggests that *O*-acetylation of SCWP may in fact be an important requirement for SLH-domain mediated adhesions in *B. anthracis*. The enzymatic attachment of an *O*-acetyl group to SCWP at this single location is likely to occur at the polymer level, as it does post-assembly on PG. The *O*-acetyl transferases/transporters PatA1 and PatA2, proposed to act on the PG substrate (Laaberki et al. 2011) are likely candidates for *O*-acetylation of SCWP, and it is noteworthy that their encoding genes reside in close proximity to *csaAB* (required for pyruvylation of SCWP) in the *B. anthracis* genome. Lastly, the occurrence of a free 2-amino group on SCWP, consistently observed at a single α-linked glucosamine residue, is likely to arise by an *N*-deacetylase, also acting on the completed polymer, as is the case for *N*-deacetylation of PG. This unique free amino modification on SCWP could also be important in SLH-domain recognition or other surface interactions. Thus, it appears that both PG and SCWP receive similar post assembly modifications with respect to *O*-acetylation and *N*-deacetylation.

The finding that only the distal three residues are structurally modified suggests a particular spatial role for SCWP, whereby the non-reducing end containing the modifications could be presented as an array, promoting ordered deposition of SLH-domain proteins. The three contiguous modified residues located at the non reducing end may prove to be an important epitope required for wall assembly in these *B. anthracis* strains, and synthetic analogs of this sequence are in preparation, for use in SLH-binding measurements and the eventual development of diagnostic reagents or vaccines.

Materials and methods

Bacillus strains

Bacillus anthracis strain CDC 684 was provided by USAMRIID. *Bacillus anthracis* Sterne strains 7702 and $34F_2$, *B. cereus* G9241, *B. cereus* 03BB87, *B. cereus* ATCC (American Type Culture Collection) 10987 and *B. cereus* ATCC 14579 were provided from the Centers for Disease Control and Prevention culture collection. Cultures were grown as described previously (Choudhury et al. 2006; Leoff et al. 2009).

Immunofluorescence labeling of B. anthracis Sterne and Ba684 vegetative cells

Following procedures described previously (Ezzell et al. 1990; Farchaus et al. 1995) *B. anthracis* Sterne $34F_2$ and Ba684 were grown on 5% sheep blood agar (SBA) medium, and a 40-µL aliquot of late logarithmic/early stationary culture was transferred to a separate vial and 1 µL of rabbit polyclonal anti-EA1 IgG (1:50) as primary antibody was added. The cell suspension was incubated for 15 min at 37°C. Post incubation, 1 mL of PBS was added and the cells pelleted by centrifugation. The supernatant was discarded and the cells were resuspended in 100 µL of PBS. Then 0.5 µL of goat anti-rabbit IgG AlexaFluor 594 conjugate (ATTO594) (1:200) secondary antibody was added and incubated for 15 min at 37 °C. The stained cells were washed with PBS then resuspended in 50 µL PBS. For microscopy, 1 µL of 1,4-Diazabicyclo (2,2,2)-octane (DABCO) quench retardant was placed on the slide followed by 1 µL of stained cell suspension, then mixed and the cover slip added.

For differential staining of *B. anthracis* Sterne cells, heart infusion broth containing 0.8% sodium bicarbonate was inoculated with *B. anthracis* Sterne $34F_2$ spores. From a two hour culture, containing primarily very young vegetative cells, 40 µL of suspension was removed and transferred to separate vial. To the cell suspension was added 10 µL of the anti-glycosyl monoclonal antibody EAII6G6-2-3 FITC-labeled IgM (1:5), followed by 1 µL addition of the rabbit polyclonal anti-EA1 IgG (1:50). The suspension was incubated for 15 min at 37°C, then washed with 1 mL of PBS and pelleted. The cells were resuspended in PBS and treated with the goat anti-rabbit IgG ATTO594 conjugate as described in the preceding paragraph and mounted with DABCO for microscopy.

Preparation of Ba684 vegetative cells for extraction

To ensure purity of vegetative cells provided for analysis, *Bacillus anthracis* CDC 684 spores were inoculated onto 5% SBA and streaked for isolation. Post incubation overnight at 35°C, the culture was inspected for homogeneous colony morphology. Approximately a 10 µL (loop) of cells from isolated colonies was removed and resuspended in 2 mL DPBS (GIBCO™ Dulbecco's Phosphate Buffered Saline (1x) liquid from Invitrogen). To six trypticase soy agar (Becton Dickenson dehydrated culture media) plates was placed 100 µL of the CDC 684 vegetative cell suspension and spread in lawn fashion with disposable L-shaped cell spreader until dry. Plates were inverted and allowed to incubate overnight at room temperature (approximately 22°C; temperature chosen to reduce spore formation). Growth was scraped from agar surface with L-spreaders, transferred to pre-weighed 50 mL Oak Ridge Teflon centrifuge tube and wet weight of cells calculated. Harvested cells were initially held frozen at −70°C prior to autoclaving and when thawed, resuspended in 10 mL of sterile deionized water then autoclaved for 30 min at 121° C. One tenth volume of the autoclaved material was sacrificed for proof of sterility and plated onto 5% sheep blood agar plates. No growth was observed after 72 h incubation at 35°C. Remaining autoclaved Ba684 vegetative cell material was stored at -70°C and subsequently shipped frozen.

Isolation of cell walls

Cell walls were prepared from cultured cells as previously described (Choudhury et al. 2006; Leoff et al. 2009), following a modified procedure (Brown 1973). The procedure yielded approx. 30–70 mg of cell walls per 100 mL of cultured cells.

Isolation and purification of SCWP

Cell wall preparations from *B. cereus* G9241, *B. cereus* 03BB87, *B. cereus* 03BB102, *B. cereus* ATCC 14579 and *B. anthracis* Sterne $34F_2$ and 7702, were treated with 48% aqueous hydrogen fluoride (HF) at 4°C for 48 h. The reaction mixtures were rotated slowly in an end-over end mixer to assist solubilization of the cell wall material. The reaction mixtures were then adjusted to pH 6.0 by rapidly transferring the mixtures directly into a predetermined amount of ammonium hydroxide solution (20% v/v) pre-cooled to −20°C. The solutions were then dialyzed at 4°C vs. deionized water for 3 days using 1000 MWCO dialysis tubing. Dialysates were concentrated by centrifugal vacuum-evaporation then subjected to ultracentrifugation (100,000 × *g*; 4°C, 4 h) to remove HF-insoluble material, yielding a supernatant containing the solubilized SCWPs (crude SCWP preparation). The HF-insoluble residue consisted of PG fragments and protein (amino acids) as determined by gas-liquid chromatography-mass spectrometry (GC-MS) analysis of the heptafluorobutyrate esters and trimethylsilyl (TMS)-methyl glycosides.

Crude SCWP was dissolved in water, filtered (0.45 µ cellulose acetate), then purified by size exclusion chromatography on Superose-12 FPLC column eluted in 50 mM ammonium acetate. The eluant was monitored by UV absorbance (215 nm) and refractive index, and fractions containing the SCWP were identified by glycosyl analysis. The SCWP fractions were pooled, lyophilized and used for NMR and immunological analyses. The yield from the normal (pathogenic) strains was typically 5 mg of purified SCWP per 40 mg of cell wall material, while the yield from Ba684 strain was approximately 1/10th, i.e. 0.5 mg per 40 mg cell walls.

Glycosyl analyses

Carbohydrate compositions of the SCWP and derived fractions were determined by preparing the TMS methyl glycosides with GC-MS (electron impact) analysis (York et al. 1985; Forsberg et al. 2003) using a 30-m DB-5 capillary column (J&W Scientific). The SCWP preparations were free of significant levels of amino acids as determined by analysis of the heptafluorobutyrate derivatives (Zanetta et al. 1999), with GC-MS analysis using a HP-5 capillary column. The absolute configuration of glycosyl residues was determined by preparing the diastereomeric TMS (±)-2-butyl glycoside derivatives (Gerwig et al. 1979), with GC-MS analysis on a DB-1 column with comparisons to authentic D-Gal, D-GlcNAc and D-ManNAc derivatives.

Nuclear magnetic resonance analyses

^{1}H spectra and all two-dimensional homo- and heteronuclear spectra of the SCWPs were recorded at 25°C on a Varian Inova 600 MHz or Varian 800 MHz spectrometer, each equipped with a 3-mm cryogenic probe, using Varian software (Varian Medical Systems, Palo Alto, CA, USA). The SCWPs released by HF treatment and purified by Superose-12 chromatography, were dissolved in 200 µL D_2O yielding clear solutions at approximately 7 mg/mL in 3 mm tubes; spectra were referenced to internal 2,2-dimethyl-2-silapentane-5-sulfonate sodium salt at δ_H 0.00 ppm, yielding HOD resonance at 4.78 ppm.

^{1}H–^{1}H COSY (Piantini et al. 1982) data were recorded in the absolute value mode with a 6.10 ppm spectral width and a matrix size of 1024 × 4096 complex points with 8 scans per increment. ^{1}H–^{1}H zTOCSY (Bax and Davis, 1985) was recorded with a mixing time of 150 ms and a matrix of 400 × 4096 at 32 scans per increment. Nuclear Overhauser effect analysis (Macura et al. 1981) was performed by phase-sensitive ^{1}H–^{1}H NOESY experiments, collected with a 150 ms mixing time and matrix size identical to that used for zTOCSY, with 64 scans per increment. Carbon chemical shifts and carbon-proton one-bond correlations were determined with a gradient-selected ^{1}H–^{13}C HSQC (Davis et al. 1991) collected in the ^{1}H-detection mode. The acquisition time was 0.2 s, and the matrix size was typically 256 × 2000 complex points, at 88 to 144 scans/increment with multiplicity distinction for primary/secondary protons. The coupling constant (1jch) was set to 150 Hz and the carbon spectral width was 110 ppm, transmitter offset 65 ppm. Phase-sensitive ^{1}H–^{13}C HMBC spectra were acquired with 256 × 2048 complex points at 96–144 scans/increment. The carbon and proton sweep widths were identical to HSQC values, and the acquisition time (t2) was 0.27 s. The HMBC transfer delay was set to 50 ms (10 Hz), and 1-bond J-filter was 150 Hz. Anomeric configurations of the glycosyl linkages were assigned from carbon-proton coupling constants ($J_{C1,H1}$) measured for the native SCWP by ^{1}H–^{13}C HSQC analysis without ^{13}C decoupling. The acquisition time was 0.6 s, collecting 128 scans per increment; the 1jch was set to 160 Hz and carbon sweep width was 80–120 ppm.

Supplementary data

Supplementary data for this article is available online at http://glycob.oxfordjournals.org/.

Funding

This work was supported in part by National Institutes of Health (R21 AI076753 to R.W.C.). The Complex Carbohydrate Research Center was supported in part by Department of Energy (DE-FG02-09ER20097).

Acknowledgements

The authors thank John Glushka for assistance with NMR analyses. The findings and conclusions in this report are those of the author(s) and do not necessarily represent the views of the Centers for Disease Control and Prevention. Patent Pending: University of Georgia Research Foundation, Inc. and US Centers for Disease Control and Prevention.

Conflict of interest

None declared.

Abbreviations

ATCC, American Type Culture Collection; Ba684, *B. anthracis* CDC 684; COSY, correlation spectroscopy; EA1, extractable antigen-1; GC-MS, gas-liquid chromatography-mass

spectrometry; HF, hydrofluoric acid; HMBC, heteronuclear multiple bond coherence spectroscopy; HSQC, heteronuclear single-quantum coherence spectroscopy; NOESY, nuclear overhauser effect spectroscopy; PG, peptidoglycan; SCWP, secondary cell wall polysaccharide; SEC, size exclusion chromatography; SLH, surface layer homology; SNP, single-nucleotide polymorphism; TMS, trimethylsilyl; TOCSY, total correlation spectroscopy.

References

Abshire TG, Brown JE, Ezzell JW. 2005. Production and validation of the use of gamma phage for identification of *Bacillus anthracis*. *J Clin Microbiol*. 43:4780–4788.

Agrawal PK. 1992. NMR spectroscopy in the structural elucidation of oligosaccharides and glycosides. *Phytochemistry*. 31:3307–3330.

Bax A, Davis DG. 1985. MLEV-17-based two-dimensional homonuclear magnetization transfer spectroscopy. *J Magn Reson*. 65:355–360.

Bhavsar AP, Brown ED. 2006. Cell wall assembly in *Bacillus subtilis*: How spirals and spaces challenge paradigms. *Mol Microbiol*. 60:1077–1090.

Brown WC. 1973. Rapid methods for extracting autolysins from *Bacillus subtilis*. *Appl Microbiol*. 25:295–300.

Candela T, Maes E, Garénaux E, Rombouts Y, Krzewinski F, Gohar M, Guérardel Y. 2011. Environmental and biofilm-dependent changes in a *Bacillus cereus* secondary cell wall polysaccharide. *J Biol Chem*. 286:31250–31262.

Cava F, De Pedro MA, Schwarz H, Henne A, Berenguer J. 2004. Binding to pyruvylated compounds as an ancestral mechanism to anchor the outer envelope in primitive bacteria. *Mol Microbiol*. 52:677–690.

Choudhury B, Leoff C, Saile E, Wilkins P, Quinn CP, Kannenberg EL, Carlson RW. 2006. The structure of the major cell wall polysaccharide of *Bacillus anthracis* is species-specific. *J Biol Chem*. 281:27932–27941.

Davis AL, Laue ED, Keeler J, Moskau D, Lohman J. 1991. Absorption mode two-dimensional NMR spectra recorded using pulse field gradients. *J Magn Reson*. 94:637–644.

De BK, Bragg SL, Sanden GN, Wilson KE, Diem LA, Marston CK, Hoffmaster AR, Barnet GA, Weyant RS, Abshire TG, et al. 2002. Two-component direct fluorescent-antibody assay for rapid identification of *Bacillus anthracis*. *Emerg Infect Dis*. 8:1060–1065.

Ekwunife FS, Singh J, Taylor KG, Doyle RJ. 1991. Isolation and purification of cell wall polysaccharide of *Bacillus anthracis* (delta Sterne). *FEMS Microbiol Lett*. 66:257–262.

Ezzell JW, Abshire TG, Little SF, Lidgerding BC, Brown C. 1990. Identification of *Bacillus anthracis* by using monoclonal antibody to cell wall galactose-*N*-acetylglucosamine polysaccharide. *J Clin Microbiol*. 28:223–231.

Farchaus JW, Ribot WJ, Downs MB, Ezzell JW. 1995. Purification and characterization of the major surface array protein from the avirulent *Bacillus anthracis* Delta Sterne-1. *J Bacteriol*. 177:2481–2489.

Forsberg LS, Choudhury B, Leoff C, Marston CK, Hoffmaster AR, Saile E, Quinn CP, Kannenberg EL, Carlson RW. 2011. Secondary cell wall polysaccharides from *Bacillus cereus* strains G9241, 03BB87, and 03BB102 causing fatal pneumonia share similar glycosyl structures with the polysaccharides from *Bacillus anthracis*. *Glycobiology*. 21:934–948.

Forsberg LS, Noel KD, Box J, Carlson RW. 2003. Genetic locus and structural characterization of the biochemical defect in the O-antigenic polysaccharide of the symbiotically deficient *Rhizobium etli* mutant, CE166: Replacement of *N*-acetylquinovosamine with its hexosyl-4-ulose precursor. *J Biol Chem*. 278:51347–51359.

Fouet A. 2009. The surface of *Bacillus anthracis*. *Mol Aspects Med*. 30:374–385.

Garegg PJ, Jansson PE, Lindberg B, Lindh F, Lönngren J, Kvarnström I, Nimmich W. 1980. Configuration of the acetal carbon atom of pyruvic acid acetals in some bacterial polysaccharides. *Carbohydr Res*. 78:127–132.

Gerwig GJ, Kamerling JP, Vliegenthart JFG. 1979. Determination of the absolute configuration of monosaccharides in complex carbohydrates by capillary G.L.C. *Carbohydr Res*. 77:1–7.

Gorin PAJ, Mazurek M, Duarte HS, Iacomini M, Duarte JH. 1982. Properties of ^{13}C-N.M.R. spectra of *O*-(1-carboxyethylidene) derivatives of methyl β-D-galactopyranoside: Models for determination of pyruvic acid acetal structures in polysaccharides. *Carbohydr Res*. 100:1–15.

Jansson P-E, Kenne L, Schweda E. 1987. Nuclear magnetic resonance and conformational studies on monoacetylated methyl D-*gluco*- and D-*galacto*-pyranosides. *J Chem Soc Perkin Trans*. 1:377–383.

Keim P, Gruendike JM, Klevytska AM, Schupp JM, Challacombe J, Okinaka R. 2009. The genome and variation of *Bacillus anthracis*. *Mol Aspects Med*. 30:397–405.

Kern J, Ryan C, Faull K, Schneewind O. 2010. *Bacillus anthracis* surface-layer proteins assemble by binding to the secondary cell wall polysaccharide in a manner that requires csaB and tagO. *J Mol Biol*. 401: 757–775.

Kern JW, Schneewind O. 2008. BslA, a pXO1-encoded adhesin of *Bacillus anthracis*. *Mol Microbiol*. 68:504–515.

Kojima N, Kaya S, Araki Y, Ito E. 1988. Pyruvic-acid-containing polysaccharide in the cell wall of *Bacillus polymyxa* AHU 1385. *Eur J Biochem*. 174:255–260.

Laaberki M-H, Pfeffer J, Clarke AJ, Dworkin J. 2011. O-acetylation of peptidoglycan is required for proper cell separation and S-layer anchoring in *Bacillus anthracis*. *J Biol Chem*. 286:5278–5288.

Leoff C, Choudhury B, Saile E, Quinn CP, Carlson RW, Kannenberg EL. 2008. Structural elucidation of the nonclassical secondary cell wall polysaccharide from *Bacillus cereus* ATCC 10987. *J Biol Chem*. 283: 29812–29821.

Leoff C, Saile E, Rauvolfova J, Quinn CP, Hoffmaster AR, Zhong W, Mehta AS, Boons GJ, Carlson RW, Kannenberg EL. 2009. Secondary cell wall polysaccharides of *Bacillus anthracis* are antigens that contain specific epitopes which cross-react with three pathogenic *Bacillus cereus* strains that caused severe disease, and other epitopes common to all the *Bacillus cereus* strains tested. *Glycobiology*. 19:665–673.

Lipkind GM, Shashkov AS, Knirel YA, Vinogradov EV, Kochetkov NK. 1988. A computer-assisted structural analysis of regular polysaccharides on the basis of ^{13}C-n.m.r. data. *Carbohydr Res*. 175:59–75.

Macura S, Huang Y, Suter D, Ernst RR. 1981. Two-dimensional chemical exchange and cross-relaxation spectroscopy of coupled nuclear spins. *J Magn Reson*. 43:259–281.

Mesnage S, Fontaine T, Mignot T, Delepierre M, Mock M, Fouet A. 2000. Bacterial SLH domain proteins are non-covalently anchored to the cell surface via a conserved mechanism involving wall polysaccharide pyruvylation. *EMBO J*. 19:4473–4484.

Mesnage S, Tosi-Couture E, Mock M, Fouet A. 1999. The S-layer homology domain as a means for anchoring heterologous proteins on the cell surface of *Bacillus anthracis*. *J Appl Microbiol*. 87:256–260.

Okinaka RT, Cloud K, Hampton O, Hoffmaster AR, Hill KK, Keim P, Koehler TM, Lamke G, Kumano S, Mahillon J, et al. 1999. Sequence and organization of pXO1, the large *Bacillus anthracis* plasmid harboring the anthrax toxin genes. *J Bacteriol*. 181:6509–6515.

Okinaka R, Price EP, Wolken SR, Gruendike JM, Chung WK, Pearson T, Xie G, Munk C, Hill KK, Challacombe J, et al. 2011. An attenuated strain of *Bacillus anthracis* (CDC 684) has a large chromosomal inversion and altered growth kinetics. *BMC Genomics*. 12:477.

Pearson T, Busch JD, Ravel J, Read TD, Rhoton SD, U'Ren JM, Simonson TS, Kachur SM, Leadem RR, Cardon ML, et al. 2004. Phylogenetic discovery bias in *Bacillus anthracis* using single-nucleotide polymorphisms from whole-genome sequencing. *Proc Natl Acad Sci USA*. 101:13536–13541.

Petersen BO, Sára M, Mader C, Mayer HF, Sleytr UB, Pabst M, Puchberger M, Krause E, Hofinger A, Duus JØ, et al. 2008. Structural characterization of the acid-degraded secondary cell wall polymer of *Geobacillus stearothermophilus* PV72/p2. *Carbohydr Res*. 343:1346–1358.

Piantini U, Sörensen OW, Ernst RR. 1982. Multiple quantum filters for elucidating NMR coupling networks. *J Am Chem Soc*. 104:6800–6801.

Schäffer C, Messner P. 2005. The structure of secondary cell wall polymers: How Gram-positive bacteria stick their cell walls together. *Microbiology*. 151:643–651.

Schäffer C, Müller N, Mandal PK, Christian R, Zayni S, Messner P. 2000. A pyrophosphate bridge links the pyruvate-containing secondary cell wall polymer of *Paenibacillus alvei* CCM 2051 to muramic acid. *Glycoconj J*. 17:681–690.

Swoboda JG, Campbell J, Meredith TC, Walker S. 2010. Wall teichoic acid function, biosynthesis, and inhibition. *Chem Bio Chem*. 11:35–45.

York WS, Darvill AG, McNeil M, Stevenson TT, Albersheim P. 1985. Isolation and characterization of plant cell walls and cell wall components. *Meth Enzymol*. 118:3–40.

Zanetta JP, Timmerman P, Leroy Y. 1999. Gas-liquid chromatography of the heptafluorobutyrate derivatives of the *O*-methyl-glycosides on capillary columns: A method for the quantitative determination of the monosaccharide composition of glycoproteins and glycolipids. *Glycobiology*. 9:255–266.

Ziegler T, Eckhardt E, Birault V. 1993. Synthetic studies toward pyruvate acetal containing saccharides. Synthesis of the carbohydrate part of the *Mycobacterium smegmatis* pentasaccharide glycolipid and fragments thereof for the preparation of neoantigens. *J Org Chem*. 58:1090–1099.